European Journal of Radiology 155 (2022) 110509

Contents lists available at ScienceDirect

European Journal of Radiology

journal homepage: www.elsevier.com/locate/ejrad

Breast dosimetry in alternative X-ray-based imaging modalities used in current clinical practices

S. Di Maria [a,*], S. Vedantham [b,c], P. Vaz [a]

[a] Centro de Ciências e Tecnologias Nucleares, Instituto Superior Técnico, Campus Tecnológico e Nuclear, Estrada Nacional 10, km 139,7, 2695-066 Bobadela LRS, Portugal
[b] Department of Medical Imaging, The University of Arizona, Tucson, AZ, USA
[c] Department of Biomedical Engineering, The University of Arizona, Tucson, AZ, USA

ARTICLE INFO

Keywords:
Breast dosimetry
Contrast Enhanced Mammography
Breast Computed Tomography
Mean Glandular Dose

ABSTRACT

In X-ray breast imaging, Digital Mammography (DM) and Digital Breast Tomosynthesis (DBT), are the standard and largely used techniques, both for diagnostic and screening purposes. Other techniques, such as dedicated Breast Computed Tomography (BCT) and Contrast Enhanced Mammography (CEM) have been developed as an alternative or a complementary technique to the established ones.

The performance of these imaging techniques is being continuously assessed to improve the image quality and to reduce the radiation dose. These imaging modalities are predominantly used in the diagnostic setting to resolve incomplete or indeterminate findings detected with conventional screening examinations and could potentially be used either as an adjunct or as a primary screening tool in select populations, such as for women with dense breasts. The aim of this review is to describe the radiation dosimetry for these imaging techniques, and to compare the mean glandular dose with standard breast imaging modalities, such as DM and DBT.

1. Background

Digital mammography (DM) and digital breast tomosynthesis (DBT) are currently considered as the gold standard in breast cancer screening of asymptomatic women. The successful deployment of such imaging tools was possible due to technological advances during the last three decades, mainly due to improvement in image quality of X-ray detectors and due to the use of more appropriate X-ray beam quality [1–6]. However, these standard breast imaging tools present some limitations. Firstly, both DM and DBT require uncomfortable breast compression.

Secondly, tissue superposition in conjunction with the relatively small difference in energy-dependent X-ray attenuation coefficients between carcinoma and fibro glandular tissue is a major challenge with DM [7,8]. DBT partly alleviates this challenge by reducing the tissue superposition [9].

The proportion of breast volume occupied by fibro glandular tissue increases with breast density, which is a known risk factor for breast cancer [10], and could also mask lesions making it more challenging to detect abnormalities in dense breasts, particularly for soft tissue lesions without microcalcifications [11]. The breast density-dependent performance of DM and DBT for screening is well-established, with substantial reduction in sensitivity for women with dense breasts [12–16].

Among non-ionizing imaging techniques, adjunctive screening with either hand-held or automated breast ultrasound in women with dense breasts is becoming increasingly common, as it has the potential to improve cancer detection rate albeit with a risk of increased false positives findings [12,17,18]. Furthermore, supplemental imaging techniques with high sensitivity and specificity, such as dynamic contrast-enhanced magnetic resonance imaging (DCE-MRI) is also practiced in select populations, such as in women with high-risk for breast cancer [19,6,20–22].

In X-ray imaging, when considering women with extremely dense breasts, typically DBT with reconstructed synthetic images are used [5]. Also, DBT in combination with DM (commonly referred to as the “combo” mode) can be used, even if did not show an improvement in cancer detection rate, and it is associated with an approximate doubling of the radiation dose [3,5].

Peer review under responsibility of If file “editor conflict of interest statement” is present in S0, please extract the information and add it as a footnote (star) to the relevant author. The sentence should read (and be amended accordingly): Given his/her role as EditorinChief/Associate Editor/Section Editor <NAME of Editor> had no involvement in the peerreview of this article and has no access to information regarding its peerreview..

* Corresponding author.
E-mail address: salvatore@ctn.tecnico.ulisboa.pt (S. Di Maria).

https://doi.org/10.1016/j.ejrad.2022.110509
Received 30 June 2022; Received in revised form 18 August 2022; Accepted 30 August 2022
Available online 6 September 2022

Nomenclature

Acronyms

BCT	Breast Computed Tomography
CB-BCT	Cone Beam Breast Computed Tomography
CEM	Contrast Enhanced Mammography
CEDM	Contrast Enhanced Digital Mammography
CEDEM	Contrast Enhanced Dual Energy Mammography
CESM	Contrast Enhanced Spectral Mammography
CF	Conversion Factors
DM	Digital Mammography
D_gN^{CT}	Normalized Glandular dose coefficients for CT
DBT	Digital Breast Tomosynthesis
EUREF	European Reference Organization for Quality Assured Breast Screening and Diagnostic Services
H-BCT	Helical Breast Computed Tomography
HEI	High Energy Image
LEI	Low Energy Image
MDCT	Multi Detector Computed Tomography
MGD	Mean Glandular Dose
MQ	Measurable Quantities

In addition to DM and DBT, emerging X-ray imaging tools have the potential to address the aforementioned limitations and can bridge the gaps for multiple clinical tasks. Two such imaging tools are dedicated Breast Computed Tomography (BCT) and Contrast Enhanced Mammography (CEM). These two imaging techniques presents some substantial difference in the irradiation setup with respect to the standard DM and DBT. BCT is based on 360° X-ray acquisitions around the uncompressed breast in pendant position and provides cross-sectional images of breast. In comparison, DBT is based on partial or limited-angle tomography of the compressed breast with the patient in upright position and the images are planes/slices along the X-ray projection. The use of contrast media in CEM and potentially with BCT, and the different spectral qualities used for image acquisition in BCT and CEM, are other factors that differentiate the imaging and dosimetric performances of these techniques from the standard DM and DBT.

In this review, the main basic concepts of breast dosimetry protocols in BCT and CEM are reviewed. The introduction to the dosimetry methodology will permit the reader to infer the dose-related quantities, such as mean glandular dose and air-kerma that are already in part used for BCT and CEM.

The dosimetric performances of BCT and CEM are compared with standard diagnostic and screening procedures (DM and DBT). Finally, the potential role of these modalities in screening programs will be also discussed.

2. Breast computed tomography (BCT)

Dedicated breast computed tomography, commonly referred to as breast CT (BCT), is an emerging modality. The first prototype dedicated BCT systems were developed in the late 1970 s [23,24]. These early-generation BCT systems were single-slice scanners using Xenon gas detectors [23,25]. The pendant breast was surrounded by a water bath and injection of iodinated contrast media was necessary due to the limited dynamic range of these detectors [23]. The images were reconstructed to 1.56 mm × 1.56 mm with slice thickness of 10 mm. In a study of 1625 women, BCT and mammography detected 94 % and 77 % of the 78 cancers [24]. However, the radiation dose was substantially higher than mammography and hence was not clinically adopted. The seminal work by *Boone et al.* [25] that demonstrated the feasibility of BCT at radiation dose comparable to mammography renewed interest in this technology [23].

Currently, there are two commercial BCT systems available. A main distinction between these two systems is related to the different irradiation geometry setup – cone-beam and fan-beam [26] (see Fig. 1). The fan-beam BCT system performs helical acquisition with photon-counting detector [27], referred to as H-BCT, and is similar to conventional whole-body multi-detector CT (MDCT). The cone-beam BCT [28–30], referred to as CB-BCT uses a large-area flat-panel detector, where the entire breast volume is imaged in a single scan. In addition, several commercial entities and academic researchers are developing and investigating clinical prototype BCT systems, including CB-BCT with various X-ray source trajectories [31–33], CB-BCT with an offset-detector [34], slot-scan BCT where a rectangular detector scans the breast along the fan-angle direction in each projection view [35], and upright BCT where women positioning is similar to DM and DBT but without breast compression [36,35].

The commercial BCT systems are mostly used for diagnostic imaging, either with or without iodinated contrast administration. Comparing CB-BCT for diagnostic imaging with diagnostic DM workup, a reader study with 18 radiologists showed improved sensitivity and non-significant change in specificity of non-contrast CB-BCT over DM-based diagnostic workup [37]. In their review, *Zhu et al* [26] report in general higher sensitivity of non-contrast BCT with respect to breast ultrasound, DBT and DM, whereas the results concerning specificity are equivocal [26,38]. Comparing DCE-MRI and contrast-enhanced BCT, sensitivity and specificity were either similar or marginally better with DCE-MRI [26,38].

3. Contrast enhanced mammography (CEM)

CEM is an emerging diagnostic technique that is being increasingly adopted clinically and can be used to improve the diagnostic accuracy with respect to other techniques used in routine breast imaging [15,39]. CEM leverages the neoangiogenesis associated “leaky vessels” to image the contrast uptake, similar to DCE-MRI. The working principle of CEM is to use a contrast material (iodine-based) that enables the acquisition of two images; one each at low and high X-ray photon energy, straddling the K-edge of iodine corresponding to 33.2 KeV [8]. It is important to remark that in literature CEM is also referred to as Contrast Enhanced Spectral Mammography (CESM), Contrast Enhanced Digital Mammography (CEDM) or Contrast Enhanced Dual-Energy Mammography (CEDEM) [15].

Contrast-enhanced spectral mammography (CESM) based on dual-energy acquisition has been introduced in the clinic. Its clinical adoption is uneven among imaging sites and will take several years before it is broadly adopted for routine diagnostic imaging [15,40]. The low-energy images (LEI) are acquired with 26–33 kVp spectra and the high-energy images (HEI) are acquired with 44–50 kVp spectra, both after contrast administration [41,40]. The anatomical information in HEI is not suitable for diagnostic purposes due to low contrast. It is used for post-processing to generate the recombined or iodine-only image that shows areas of contrast enhancement. In clinical practice, the radiologist reads the LEI and recombined (or iodine-enhanced) images [15]. The total breast compression time of a single exposure depends on breast composition and thickness, and the time could vary from 2 s to 20 s. Several studies indicate comparable or superior sensitivity and specificity of CEM compared to DM, especially in women with dense breasts [42].

4. Radiation dosimetry

Given the potential of these two tools, primarily for diagnostic imaging and possibly for screening, the aim of this review is to discuss the mean glandular dose (MGD) from these imaging modalities. For all modalities and variations in technology, breast dosimetry follows the general formalism described by Eq. (1) of [1] that is reported below for completeness:

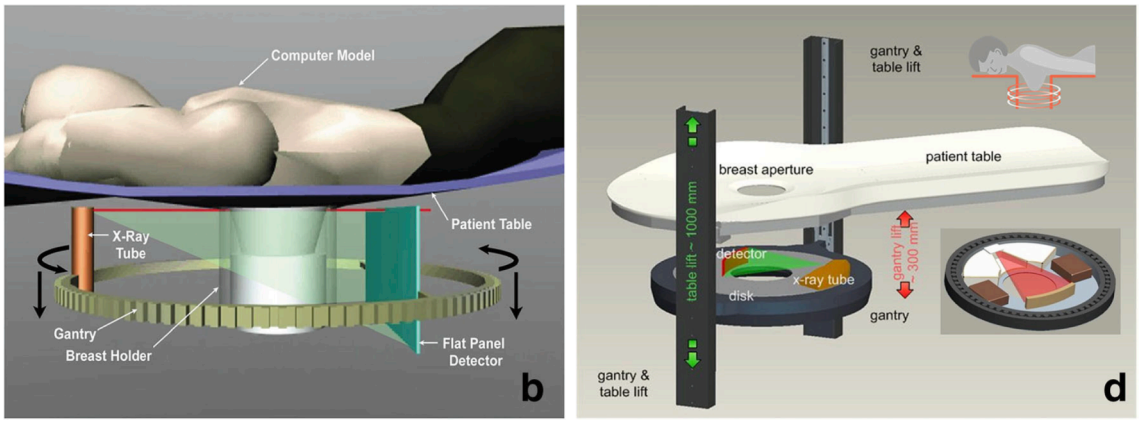

Fig. 1. b: Koning breast CT: women lies prone with one breast suspended through a tabletop opening into the imaging field, the X-ray tube and the flat-panel detector rotate 360° around the breast for a single continuous acquisition. **d:** Advanced breast CT: women lies in a prone position on the tabletop, the examined breast is positioned in an aperture without compression, the gantry moves up and down independently allowing for spiral acquisition (Figure reprinted under permission of European Radiology journal [26]).

$$Dose_{organ} = CF \bullet MQ \quad (1)$$

Where the conversion factor (CF) depends on the geometrical setup (beam source, energy, and distance source-target) used for image acquisition and on the breast model (shape, size and composition of the breast). The CFs are obtained from Monte Carlo simulations. The measurable quantity (MQ) depends on the modality/technology and varies in terms of the location of measurement. The location at which the air Kerma is measured in BCT differs from DM and DBT; in DM and DBT, the air Kerma is measured at skin entrance, whereas in BCT the air Kerma is measured at the axis-of-rotation (also referred to as isocenter). Most breast cancers begin in the glands or ductal epithelium. Hence, the dose to the breast (organ dose) is reported using the Mean Glandular Dose (MGD) metric, which allocates the radiation dose to the "at-risk" fibroglandular tissue.

4.1. Dosimetry in CB-BCT

In CB-BCT, the X-ray beam width along the chest-wall to nipple direction (cone angle) is approximately 20 cm. This extent is larger than the 10 cm ionization chamber commonly used during quality control audits of whole-body MDCT systems. Thus, in each projection, the ionization chamber is completely in the X-ray field-of-view. Hence, the measurable quantity (MQ) is the air Kerma (AK) in units of mGy. This is a free-in-air measurement without any phantom and is measured at the axis-of-rotation (isocenter).

The CF is derived from Monte Carlo simulations for a specified breast model and is referred to as normalized glandular dose coefficient (D_gN^{CT}, in units of mGy/mGy). Unlike digital mammography and DBT, the breast is not compressed during a CB-BCT exam. Hence, for determining the D_gN^{CT} from Monte Carlo simulations, the breast is modeled as a semi-ellipsoid with the minor axis corresponding to the radius of the semi-ellipsoidal breast at the chest wall and the major axis representing the chest wall to nipple distance. Data from clinical studies [31,32] indicate that the average radius of the breast at the chest-wall is approximately 7 cm and the average chest-wall to nipple distance is approximately 10.5 cm. The thickness of skin comprising epidermis and dermis (and excluding subcutaneous fat) measured from CB-BCT is approximately 1.45 mm [43,44]. The breast is modeled as a homogenous mixture of adipose and fibroglandular tissue. Data from clinical studies using CB-BCT show that the glandularity or fibroglandular weight fraction for an average breast is approximately 15 % [45,32] and differs from the 50 % glandularity assumed for breast dosimetry in early studies. During Monte Carlo simulations to determine D_gN^{CT}, the semi-ellipsoidal breast model is aligned with the axis of rotation, corresponding to the location of air Kerma measurement. The energy deposited to the breast is apportioned based on the glandularity used in the breast model.

D_gN^{CT} for CB-BCT have been reported by several research groups to reflect the imaging geometry, tube voltage and target/filter combination. In terms of imaging geometry, these include studies reporting the D_gN^{CT} coefficients for the typical circular trajectory of the X-ray source [31,46], for the circle-plus-line X-ray source trajectory [47], and for offset-detector geometry [48]. These studies cover the range of tube voltages and target/filter combinations used in various BCT systems and prototypes. While all BCT systems currently use tungsten target, the X-ray beam filter can be Al, Cu, combination of Al and Cu, or K-edge filters such as La and Ce [49] to provide a quasi-monochromatic beam.

The metric for reporting the dose to the breast is the Mean Glandular Dose (MGD) and is the product of the conversion factor (D_gN^{CT}) and the measured air Kerma. The ionization chamber/radiation dosimeter may need additional calibration by an accredited laboratory as most of the current breast CT systems operate in the range of 49–60 kV, which is not in the range used commonly in mammography, radiography or whole-body MDCT.

4.2. Dosimetry in H-BCT

In standard CT dosimetry, the concept of computed tomography dose index (CTDI) is well established. This metric provides a technical measure of scanner performance and is routinely performed as part of quality control audits. For an axial scan:

$$CTDI_{\infty} = \frac{1}{C_z}\int_{-\infty}^{+\infty} D(z)dz \quad (2)$$

where, $D(z)$ is the dose distribution along the z-axis and C_z is the collimation width, also referred to as the beam width, at the axis-of-rotation. The z-axis is the line perpendicular to the rotational plane of the X-ray source. For n slices, each with slice thickness of T mm, $C_z = nT$. The CTDI assessed with a 100 mm long pencil ionization chamber is:

$$CTDI_{100} = \frac{1}{C_z}\int_{-50mm}^{+50mm} D(z)dz \quad (3)$$

Further extensions include the $CTDI_w$ that weights the measurements performed at the center and periphery of the specified phantoms, and the $CTDI_{vol}$ that extends the method to helical acquisition.

It is well recognized that the CTDI metrics do not represent the dose to organ, but a dose index for monitoring system performance. However,

the CTDI free-in-air measurement, *i.e.,* without any phantom, can be combined with Monte Carlo simulations to obtain the MGD. The $CTDI_{free,air}$ is:

$$CTDI_{free,air} = \frac{1}{\mathrm{MIN}(nT, 100mm)} \int_{-50mm}^{+50mm} D(z)dz \quad (4)$$

In H-BCT, the beam width along the chest-wall to nipple direction is 40 mm or less, and is smaller than the 100 mm long ionization chamber. Hence, the normalization in Eqn. (4) is the beam width. Monte Carlo simulations are used to determine the CTDI free-in-air to MGD conversion factors by considering the X-ray spectrum used for data acquisition, imaging geometry, and scan trajectory.

4.3. Dosimetry in CEM

Concerning breast dosimetry, the formalism for MGD estimation in CEM follows Eq. (1). *Dance et al.* [50] published several conversion factors for use in CEM. The dosimetric formalism is the same as DM and DBT, the difference being that the tabulated values reflect the X-ray spectra used. The conversion factors are calculated for voltages between 40 and 50 kV filtered by copper [50]. In this study no consideration was done for the effect of iodine contrast media on the breast dose, since less than 5 % reduction in the transmission of X-rays through the breast is expected.

5. Mean glandular dose (MGD) from clinical studies

The MGD from these modalities needs to be considered in the context of the clinical application. For screening, the MGD needs to be within the limits specified by regulatory authorities and preferably similar to or lower than the standard DM and DBT. It is important to recognize the limits specified by regulatory authorities are for a single acquisition either for a standard breast or for specified compressed breast thickness. The United States Food and Drug Administration (US FDA) [51] specifies a limit of 3 mGy for a standard 4.3 cm thick phantom, which approximates a 5 cm thick breast. EUREF protocol specifies an acceptance limit of 2.5 mGy for 4.5 cm thick PMMA, which approximates a 5.3 cm thick compressed breast [52]. It is important to recognize the MGD would increase substantially for thicker compressed breasts. For screening, it is common to acquire two standard views. If the modality intends to replace these two standard views, then acceptance level is interpreted as twice the regulatory limit. For diagnostic workup using DM and DBT, the number of views, and consequently the MGD, would vary individually based on clinical need.

5.1. Mean glandular dose (MGD) from CB-BCT and H-BCT

A clinical study using CB-BCT aimed at maintaining the MGD comparable to standard 2-view mammography reported a MGD value of 6 mGy [28]. For a quasi-monochromatic beam with Ce filter, absorbed radiation dose measurements using radiochromic film reported that approximately 4.5 mGy dose is achievable [53]. Thus, it is possible for BCT to achieve dose values comparable to standard 2-view mammography, which could pave the way to its transition for screening applications.

For non-contrast CB-BCT targeting diagnostic imaging (not screening), the goal is to maintain the radiation dose to be comparable to a diagnostic mammography workup. Paired studies with DM and non-contrast CB-BCT for diagnostic workup show that the MGD from non-contrast BCT (13.9 ± 4.6 mGy) is comparable to the MGD from diagnostic DM workup (12.4 ± 6.3 mGy) and with a smaller range [54]. Progressive improvements in BCT technology have further reduced the MGD to 7.2 ± 2.6 mGy [16] and subsequently to 5.85 mGy [55] for diagnostic imaging.

For contrast-enhanced BCT, ty-pically-two scans are performed; one prior to and one after administration of iodinated contrast media that is similar to temporal subtraction method used in early versions of CEM. Thus, the MGD from contrast-enhanced BCT will be approximately double of non-contrast BCT. For contrast-enhanced CB-BCT, an initial study reported MGD of 8–32 mGy [56,55]. A subsequent study reported MGD of 11.7–15 mGy. Another study reported that the MGD can be reduced to 5.9 mGy by foregoing the pre-contrast scan and acquiring only the post-contrast CB-BCT, without loss of diagnostic accuracy [57]. In the case of contrast-enhanced H-BCT, if the spectral discrimination capabilities of the photon counting detector technology are leveraged then one post-contrast acquisition would be sufficient [58].

5.2. Mean glandular dose (MGD) from CEM

Breast tumor growth is accompanied by the development of vasculature, which can be of poor quality and can leak. For this reason it was proposed that CEM could have the potential to provide both functional information and improved visualization of the morphology of a cancer by reducing the visualization of the overlaying and surrounding tissues in the image [50,59].

The first attempt in using CEM was performed by using a digital subtraction technique [40]. The approach consisted in acquiring an image before contrast medium administration and another after the contrast administration. However this approach was soon abandoned due to difficulties in co-registration of unenhanced and contrast-enhanced images [60]. Successively, contrast-enhanced spectral mammography (CESM) has been introduced, based on dual-energy breast exposure, about 26–33 kVp for low energy images (LEI) and 44–50 kVp for high energy images (HEI), both after contrast administration, so that the pre-contrast exposure was no longer needed [40].

Fusco et al. [39] compared the MGD from DBT and CEM and concluded that the variability in breast compression affecting the compressed breast thickness (CBT) could influence the MGD in CEM. The MGD from both techniques met the European Reference Organization for Quality Assured Breast Screening and Diagnostic Services (EUREF) [52] recommendations for maximum dose in DM (MGD less than 2 mGy for a 4.5 cm breast thickness and less than 6.5 mGy for a 9 cm breast thickness). As expected, there were significant differences in MGD for both CEM and DBT between the two standard views. *Gennaro et al.* [61] reported population-based studies of the MGD from CEM in two hospital units. The MGD from CEM differed by 6.2 % between the two centers and were attributable to the study populations' characteristics and to manufacturing differences between the two systems. Also, the MGD from CEM was about 30 % higher than that of standard DM. This MGD increase is comparable to that observed for DBT (with respect to DM) [61]. On average 70 % of the total dose is from the LEI, and the remaining 30 % is from the HEI [61]. *Hendrick* [62] also reported a small increase in MGD for CEM relative to DM or DBT.

5.3. MGD distribution in breast volume

When comparing dosimetric differences among different techniques, such as DM, DBT and BCT, in addition to the MGD values comparison, it is important also to consider the MGD distribution inside the breast volume. Specifically, the absorbed dose variation within the breast volume may influence radiation-induced cancer risk [63]. The MGD gradient for DM or DBT is substantially higher than in BCT [64,65], mainly due to the imaging geometry in 2D vs 3D acquisition, and partly due to the difference in spectral quality (higher X-ray energy are used in BCT). For DM and DBT, the absorbed dose is higher at skin entrance, whereas the MGD distribution is more uniform in CB-CBCT [64] (see Fig. 2). The MGD variation over the breast volume ranged 65 % – 140 % for CB-BCT, whereas it was 15 % – 400 % for DM [65] In addition, it is important to remark that, for a given imaging modality, the absorbed dose distribution is also dependent by the glandular fraction distribution and breast thickness. MGD distribution for CEM is expected to be similar

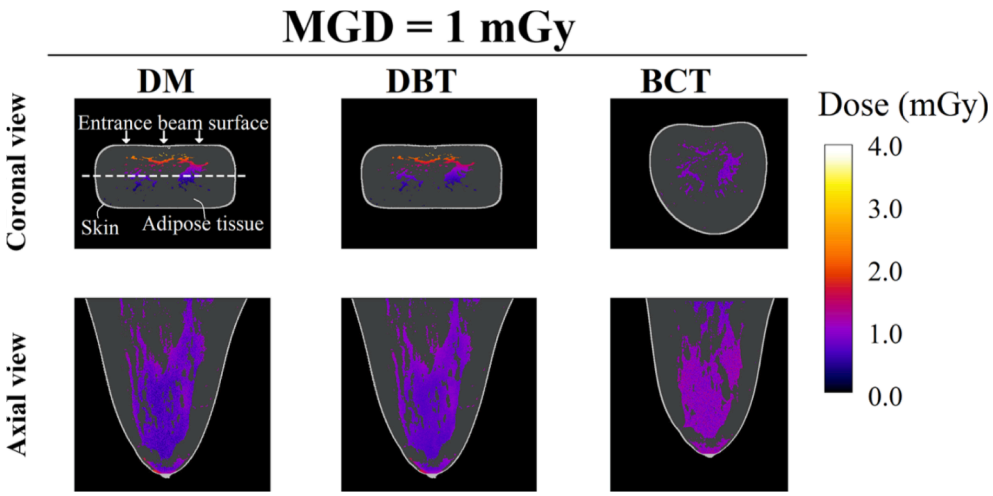

Fig. 2. Coronal and middle axial slices of the glandular dose distributions in DM, DBT and BCT for breast phantom. The dose distributions are embedded in the corresponding slices of the digital phantoms. Compressed breast thickness = 66 mm; equivalent diameter at the center of mass of the uncompressed phantom = 109 mm; glandular fraction by weight of the uncompressed phantom = 21 %. It was assumed a MGD of 1 mGy (Figure reprinted under permission of Physica Medica journal [64]).

as DM, since mostly the same irradiation setup of DM is used for CEM.

6. Closing remarks

CEM and BCT are two promising diagnostic techniques. For diagnostic imaging, the performance of CEM and BCT are comparable or, in some cases, superior to the standard imaging tools (DM and DBT). For diagnostic imaging, the MGD from CEM and BCT are comparable to DM and DBT-based diagnostic workup. The number of images for diagnostic depends by the specific clinical task. Considering for example an average number of about four views for diagnostic purposes with standard DM, and one-view for BCT, the MGD of BCT and DM are comparable or less [54].

In order to understand the MGD from BCT and CEM examinations for potential use in screening programs, the MGD values were compared with standard modalities (DM and DBT) in Fig. 3. The EUREF MGD limit for one-view mammography acquisition [52] for an equivalent breast thickness of 5.3 cm is also shown. The data reported for DM, DBT and CB-BCT were taken from [29,55], the data for H-BCT from [27] and the data for CEM from [62]. It is important to remark that such as comparison is only indicative, since for the MGD can vary among screening protocols, such as DM, DBT, or the combination of DM and DBT, and is dependent on breast thickness and glandularity. Also, a strict comparison of MGD should be performed taking into account the imaging performance of each modality.

The MGD values reported refer to a breast thickness (performed mostly in phantom measurements) interval among 4.5 cm and 6 cm. The data reported are therefore subject to uncertainties related to breast thicknesses, glandularity and exposure parameters. Nevertheless, the data reported in Fig. 3 allow for some context about the possibility of introducing new technologies in breast screening programs. It is important to stress that the data of Fig. 3 (DBT, DM and CEM) are for one-view acquisition. Considering only one-view acquisition, the MGD interval for CEM already fall almost inside the EUREF MGD limits. *Gennaro et al.* [61] showed that dose concerns for CEM should not be an obstacle for future clinical implementation, both for diagnostic

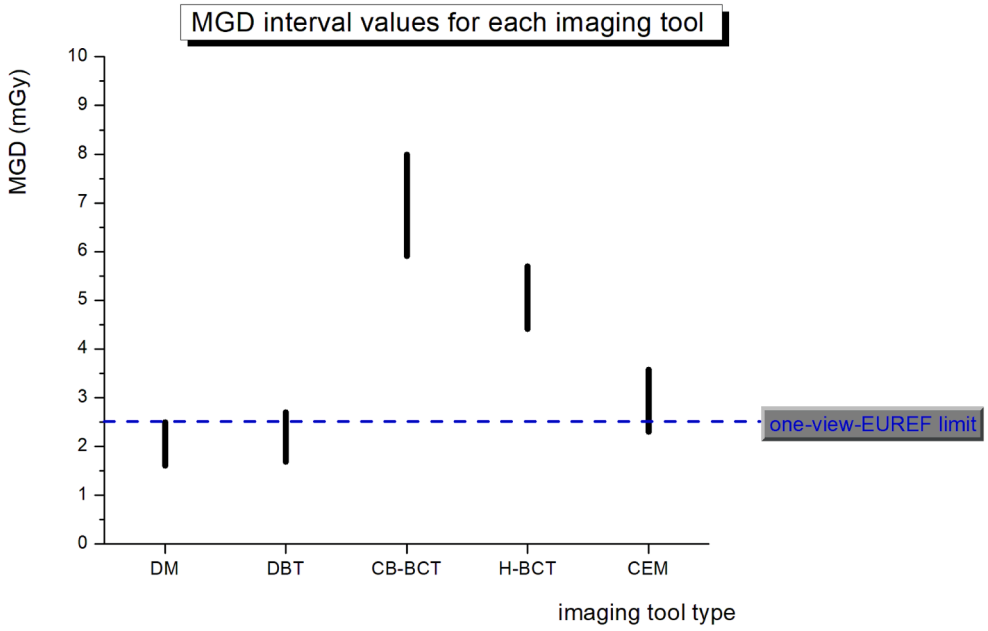

Fig. 3. MGD interval values for each imaging tool, as reported in literature [55,29,62]. For DM, DBT and CEM, the MGD values are for one-view acquisition. For CB-BCT and H-BCT, the MGD values are for a single scan. Blue line represents the MGD maximum value, as suggested by EUREF [52], permitted for one-view image acquisition in mammography in the case of an equivalent breast thickness of 5.3 cm.

evaluation of recalled subjects and for screening of specific populations. MGD values of H-BCT and CB-BCT are higher than the DBT, DM, CEM and EUREF limits. However, most screening programs use two view-acquisitions for DM and DBT. Thus, the MGD values associated with a single H-BCT or CB-BCT scan are comparable with two-view acquisitions performed with DM and DBT.

However, concerning BCT dosimetry, a further effort will be necessary in order to harmonize the dosimetric protocols. For example, significant differences in dose estimations could be found because of the methods used in H-BCT and CB-BCT. Specifically, the methods to calculate air-kerma to dose conversion coefficients, some bias in MGD estimation could be introduced when using different breast models. Also, the choice of dosimeter (ionization chamber vs solid-state detector) used to measure air-kerma [66,67,27] could introduce variability [68,69].

Concerning dosimetric issues in CEM, the MGD value associated to this imaging tool is quite close to those of DM and DBT, as shown in Fig. 3. However, further studies could be focused on the dose delivered to the breast in the presence of a contrast agent. The *Dance et al.* [50] dosimetric formalism takes into account only the difference of the X-ray energy spectra, when performing CEM with respect to DM or DBT (performed at lower energies). In CESM the two images are acquired both after iodine administration, and for this reason, even for the LE spectrum, the energy absorption in proximity of the contrast material could be significant.

Finally, dosimetric performances of BCT and CEM, as reported in this review, are already close to the standard modalities (DM and DBT). Also, given their respective benefits (functional information plus morphological information for CEM, complete 3D information for BCT), CEM and BCT could potentially be of value for other clinical applications including breast cancer screening in select populations, such as for women with high life-time risk, or for women with dense breasts [29,70,61]. In order to translate these techniques for screening, the MGD needs to meet regulatory requirements. For CB-BCT, numerous techniques including sparse view acquisition and/or short-scan acquisition in conjunction with advanced statistical image reconstruction and deep-learning assisted reconstruction are being explored.

Declaration of Competing Interest

The authors declare that they have no known competing financial interests or personal relationships that could have appeared to influence the work reported in this paper.

Acknowledgements

This work was supported in part by National Cancer Institute (NCI) of the National Institutes of Health (NIH) grants R01 CA199044 and R01 CA241709. The contents are solely the responsibility of the authors and do not necessarily reflect the official views of the NCI or the NIH.

References

[1] S. Di Maria, S. Vedantham, P. Vaz, X-ray dosimetry in breast cancer screening: 2D and 3D mammography, Eur. J. Radiol. 151 (2022) 110278.
[2] D.R. Dance, I. Sechopoulos, Dosimetry in x-ray-based breast imaging, Phys. Med. Biol. 61 (19) (2016) R271–R304.
[3] B.H. Østerås, A.C.T. Martinsen, R. Gullien, P. Skaane, Digital Mammography versus Breast Tomosynthesis: Impact of Breast Density on Diagnostic Performance in Population-based Screening, Radiology 293 (1) (2019) 60–68.
[4] S. Vedantham, A. Karellas, G.R. Vijayaraghavan, D.B. Kopans, Digital Breast Tomosynthesis: State of the Art, Radiology 277 (3) (2015) 663–684.
[5] P. Skaane, A.I. Bandos, L.T. Niklason, S. Sebuødegård, B.H. Østerås, R. Gullien, D. Gur, S. Hofvind, Digital Mammography versus Digital Mammography Plus Tomosynthesis in Breast Cancer Screening: The Oslo Tomosynthesis Screening Trial, Radiology 291 (1) (2019) 23–30.
[6] E.A. Rafferty, M.A. Durand, E.F. Conant, D.S. Copit, S.M. Friedewald, D.M. Plecha, D.P. Miller, Breast Cancer Screening Using Tomosynthesis and Digital Mammography in Dense and Nondense Breasts, JAMA 315 (16) (2016) 1784.
[7] P.C. Johns, M.J. Yaffe, X-ray characterisation of normal and neoplastic breast tissues, Phys. Med. Biol. 32 (6) (1987) 675–695.
[8] "National Institute of Standars and Technology," May 2021. [Online]. Available: https://www.nist.gov/pml/x-ray-mass-attenuation-coefficients.
[9] L.T. Niklason, B.T. Christian, L.E. Niklason, D.B. Kopans, D.E. Castleberry, B. H. Opsahl-Ong, C.E. Landberg, P.J. Slanetz, A.A. Giardino, R. Moore, D. Albagli, M. C. DeJule, P.F. Fitzgerald, D.F. Fobare, B.W. Giambattista, R.F. Kwasnick, J. Liu, S. J. Lubowski, G.E. Possin, J.F. Richotte, C.Y. Wei, R.F. Wirth, Digital tomosynthesis in breast imaging. Radiology 205 (2) (1997) 399–406.
[10] N.F. Boyd, H. Guo, L.J. Martin, L. Sun, J. Stone, E. Fishell, R.A. Jong, G. Hislop, A. Chiarelli, S. Minkin, M.J. Yaffe, Mammographic Density and the Risk and Detection of Breast Cancer, N Engl J Med 356 (3) (2007) 227–236.
[11] A.E. Burgess, F.L. Jacobson, P.F. Judy, Human observer detection experiments with mammograms and power-law noise, Med. Phys. 28 (4) (2001) 419–437.
[12] T.M. Kolb, J. Lichy, J.H. Newhouse, Comparison of the Performance of Screening Mammography, Physical Examination, and Breast US and Evaluation of Factors that Influence Them: An Analysis of 27,825 Patient Evaluations, Radiology 225 (1) (2002) 165–175.
[13] E.D. Pisano, C. Gatsonis, E. Hendrick, M. Yaffe, J.K. Baum, S. Acharyya, E. F. Conant, L.L. Fajardo, L. Bassett, C. D'Orsi, R. Jong, M. Rebner, Diagnostic Performance of Digital versus Film Mammography for Breast-Cancer Screening, N Engl J Med 353 (17) (2005) 1773–1783.
[14] E. Pisano, C. Gatsonis, E. Hendrick, M. Yaffe, J. Baum, S. Acharyya, E. Conant, L. Fajardo, L. Bassett, C. D'Orsi, R. Jong and R. M, "Correction to Diagnostic Performance of Digital versus Film Mammography for Breast-Cancer Screening," The New England Journal of Medicine, October 2006. DOI: 10.1056/NEJMx060061.
[15] M.S. Jochelson, M.B.I. Lobbes, Contrast-enhanced Mammography: State of the Art, Radiology 299 (1) (2021) 36–48, https://doi.org/10.1148/radiol.2021201948. PMID: 33650905 PMCID: PMC7997616.
[16] S. Wienbeck, J. Uhlig, S. Luftner-Nagel, A. Zapf, A. Surov, E. Von Fintel, V. Stajnke, J. Lotz, U. Fischer, The role of cone-beam breast-CT for breast cancer detection relative to breast density, Eur. Radiol. 27 (12) (2017) 5185–5195, https://doi.org/10.1007/s00330-017-4911-z. PMID: 28677053.
[17] W.A. Berg, Combined Screening With Ultrasound and Mammography vs Mammography Alone in Women at Elevated Risk of Breast Cancer, JAMA 299 (18) (2008) 2151.
[18] R.F. Brem, L. Tabár, S.W. Duffy, M.F. Inciardi, J.A. Guingrich, B.E. Hashimoto, M. R. Lander, R.L. Lapidus, M.K. Peterson, J.A. Rapelyea, S. Roux, K.J. Schilling, B. A. Shah, J. Torrente, R.T. Wynn, D.P. Miller, Assessing Improvement in Detection of Breast Cancer with Three-dimensional Automated Breast US in Women with Dense Breast Tissue: The SomoInsight Study, Radiology 274 (3) (2015) 663–673.
[19] D.A. Sippo, K.S. Burk, S.F. Mercaldo, G.M. Rutledge, C. Edmonds, Z. Guan, K. S. Hughes, C.D. Lehman, Performance of Screening Breast MRI across Women with Different Elevated Breast Cancer Risk Indications, Radiology 292 (1) (2019) 51–59.
[20] U. Bick, C. Engel, B. Krug, W. Heindel, E.M. Fallenberg, K. Rhiem, D. Maintz, M. Golatta, D. Speiser, D. Rjosk-Dendorfer, I. Lämmer-Skarke, F. Dietzel, K.W. F. Schäfer, E. Leinert, S. Weigel, S. Sauer, S. Pertschy, T. Hofmockel, A. Hagert-Winkler, K. Kast, A. Quante, A. Meindl, M. Kiechle, M. Loeffler, R.K. Schmutzler, High-risk breast cancer surveillance with MRI: 10-year experience from the German consortium for hereditary breast and ovarian cancer, Breast Cancer Res Treat 175 (1) (2019) 217–228.
[21] M. Dietzel, P.A.T. Baltzer, K. Schön, W.A. Kaiser, MR-mammography: high sensitivity but low specificity? New thoughts and fresh data on an old mantra, Eur. J. Radiol. 81 (2012) S30–S32.
[22] C. Grippo, P. Jagmohan, T.H. Helbich, P. Kapetas, P. Clauser, P.A.T. Baltzer, Correct determination of the enhancement curve is critical to ensure accurate diagnosis using the Kaiser score as a clinical decision rule for breast MRI, Eur. J. Radiol. 138 (2021) 109630.
[23] A. Sarno, G. Mettivier, P. Russo, Dedicated breast computed tomography: Basic aspects: Breast computed tomography with dedicated scanners, Med. Phys. 42 (6Part1) (2015) 2786–2804.
[24] C. H. Chang, J. L. Sibala, S. L. Fritz, S. Dwye 3rd, A. W. Templeton, F. Lin and W. R. Jewell, "Computed tomography in detection and diagnosis of breast cancer," Cancer 46(4) (1980) 939-46. DOI: 10.1002/1097-0142(19800815)46:4+<939::aid-cncr2820461315>3.0.co;2-l.
[25] J.M. Boone, T.R. Nelson, K.K. Lindfors, J.A. Seibert, Dedicated Breast CT: Radiation Dose and Image Quality Evaluation, Radiology 221 (3) (2001) 657–667.
[26] Y. Zhu, A.M. O'Connell, Y. Ma, A. Liu, H. Li, Y. Zhang, X. Zhang, Z. Ye, Dedicated breast CT: state of the art—Part I. Historical evolution, European Radiology 32 (3) (2022) 1579–1589, https://doi.org/10.1007/s00330-021-08179-z. PMID: 34342694.
[27] N. Berger, M. Marcon, N. Saltybaeva, W.A. Kalender, H. Alkadhi, T. Frauenfelder, A. Boss, Dedicated Breast Computed Tomography With a Photon-Counting Detector: Initial Results of Clinical In Vivo Imaging, Invest. Radiol. 54 (7) (2019) 409–418.
[28] K.K. Lindfors, J.M. Boone, T.R. Nelson, K. Yang, A.L.C. Kwan, D.F. Miller, Dedicated Breast CT: Initial Clinical Experience, Radiology 246 (3) (2008) 725–733.
[29] A.M. O'Connell, A. Karellas, S. Vedantham, The Potential Role of Dedicated 3D Breast CT as a Diagnostic Tool: Review and Early Clinical Examples, Breast J 20 (6) (2014) 592–605.
[30] S. Vedantham, A.M. O'Connell, L. Shi, A. Karellas, A.J. Huston, K.A. Skinner, Dedicated Breast CT: Feasibility for Monitoring Neoadjuvant Chemotherapy Treatment, Journal of Clinical Imaging Science (2014) 4–64, https://doi.org/10.4103/2156-7514.145867. PMCID: PMC4278089;PMID: 25558431.

[31] J.M. Boone, N. Shah, T.R. Nelson, A comprehensive analysis of DgNCT coefficients for pendant-geometry cone-beam breast computed tomography, Med. Phys. 31 (2) (2004) 226–235.
[32] S. Vedantham, L. Shi, A. Karellas, A.M. O'Connell, Dedicated breast CT: Fibroglandular volume measurements in a diagnostic population: Fibroglandular volume in breast CT, Med. Phys. 39 (12) (2012) 7317–7328.
[33] J.P. Shah, S.D. Mann, R.L. McKinley, M.P. Tornai, Characterization of CT Hounsfield Units for 3D acquisition trajectories on a dedicated breast CT system, XST 26 (4) (2018) 535–551.
[34] H.W. Tseng, A. Karellas, S. Vedantham, Cone-beam breast CT using an offset detector: effect of detector offset and image reconstruction algorithm, Phys. Med. Biol. 67 (8) (2022) 085008.
[35] P. Ghazi, S. Youssefian, T. Ghazi, A novel hardware duo of beam modulation and shielding to reduce scatter acquisition and dose in cone-beam breast CT, Medical Physics 49 (1) (Jan 2022) 169–185, https://doi.org/10.1002/mp.15374. PMID: 34825715.
[36] H. Tseng, A. Karellas, S. Vedantham, Sparse-view, short-scan, dedicated cone-beam breast computed tomography: image quality assessment, Biomedical Physics & Engineering Express (2020), https://doi.org/10.1088/1361-648X/abd739. PMID: 33377758 PMCID: PMC8004539.
[37] E. Cole, A. Campbell, S. Vedantham, E. Pisano and A. Karellas, "Clinical Performance of Dedicated Breast Computed Tomography in Comparison to Diagnostic Digital Mammography," Assembly and Annual Meeting of the Radiological Society of North America (RSNA), 2015.
[38] Y. Zhu, A.M. O'Connell, Y. Ma, A. Liu, H. Li, Y. Zhang, X. Zhang, Z. Ye, Dedicated breast CT: state of the art—Part II. Clinical application, European Radiology 32 (4) (2022) 2286–2300, https://doi.org/10.1007/s00330-021-08178-0. PMID: 34476564.
[39] R. Fusco, N. Raiano, C. Raiano, F. Maio, P. Vallone, M. Mattace Raso, S.V. Setola, V. Granata, M.R. Rubulotta, M.L. Barretta, T. Petrosino, A. Petrillo, Evaluation of average glandular dose and investigation of the relationship with compressed breast thickness in dual energy contrast enhanced digital mammography and digital breast tomosynthesis, Eur. J. Radiol. 126 (2020) 108912.
[40] M. Zanardo, A. Cozzi, R.M. Trimboli, O. Labaj, C.B. Monti, S. Schiaffino, L. A. Carbonaro, F. Sardanelli, Technique, protocols and adverse reactions for contrast-enhanced spectral mammography (CESM): a systematic review, Insights into Imaging (2019) 10–76, https://doi.org/10.1186/s13244-019-0756-0, PMCID: PMC6677840. PMID: 31376021.
[41] J.M. Lewin, P.K. Isaacs, V. Vance, F.J. Larke, Dual-Energy Contrast-enhanced Digital Subtraction Mammography: Feasibility, Radiology 229 (1) (2003) 261–268.
[42] B.K. Patel, M.B.I. Lobbes, J. Lewin, Contrast Enhanced Spectral Mammography: A Review, Seminars in Ultrasound, CT and MRI 39 (1) (2018) 70–79.
[43] S.-Y. Huang, J.M. Boone, K. Yang, A.L.C. Kwan, N.J. Packard, The effect of skin thickness determined using breast CT on mammographic dosimetry: The evaluation of breast thickness using breast CT, Med. Phys. 35 (4) (2008) 1199–1206.
[44] L. Shi, S. Vedantham, A. Karellas, A. O'Connell, Skin thickness measurements using high-resolution flat-panel cone-beam dedicated breast CT, Med. Phys. 40 (3) (2013), 031913.
[45] M.J. Yaffe, J.M. Boone, N. Packard, O. Alonzo-Proulx, S.-Y. Huang, C.L. Peressotti, A. Al-Mayah, K. Brock, The myth of the 50-50 breast: Myth of 50-50 breast, Med. Phys. 36 (12) (2009) 5437–5443.
[46] S.C. Thacker, S.J. Glick, Normalized glandular dose (DgN) coefficients for flat-panel CT breast imaging, Phys. Med. Biol. 49 (24) (2004) 5433–5444.
[47] S. Vedantham, L. Shi, A. Karellas, F. Noo, Dedicated breast CT: radiation dose for circle-plus-line trajectory: Breast CT dose for circle-plus-line, Med. Phys. 39 (3) (2012) 1530–1541.
[48] H.W. Tseng, A. Karellas, S. Vedantham, Radiation dosimetry of a clinical prototype dedicated cone-beam breast CT system with offset detector, Med. Phys. 48 (3) (2021) 1079–1088.
[49] R.L. McKinley, M.P. Tornai, E. Samei, M.L. Bradshaw, Simulation study of a quasi-monochromatic beam for X-ray computed mammotomography, Medical Physics. PMID 31 (4) (2004) 800–813.
[50] D.R. Dance, K.C. Young, Estimation of mean glandular dose for contrast enhanced digital mammography: Factors for use with, Physics inMedicine and Biology 59 (2014) 2127–2137, https://doi.org/10.1088/0031-9155/59/9/2127. PMID: 24699200.
[51] "Food and Drug Administration," May 2021. [Online]. Available: https://www.fda.gov/.
[52] EUREF, "European Reference Organization for Quality Assured Breast Screening and Diagnostic Services," 26 April 2022. [Online]. Available: https://www.euref.org/organisation/contact-information. [Accessed 26 April 2022].
[53] D.J. Crotty, S.L. Brady, D.C. Jackson, G.I. Toncheva, C.E. Anderson, T. T. Yoshizumi, M.P. Tornai, Evaluation of the absorbed dose to the breast using radiochromic film in a dedicated CT mammotomography system employing a quasi-monochromatic x-ray beam: Breast dosimetry using radiochromic film and computed tomography, Med. Phys. 38 (6Part1) (2011) 3232–3245.
[54] S. Vedantham, L. Shi, A. Karellas, A.M. O'Connell, D.L. Conover, Personalized estimates of radiation dose from dedicated breast CT in a diagnostic population and comparison with diagnostic mammography, Phys. Med. Biol. 58 (22) (2013) 7921–7936.
[55] S. Wienbeck, U. Fischer, S. Luftner-Nagel, J. Lotz, J. Uhlig, Contrast-enhanced cone-beam breast-CT (CBBCT): clinical performance compared to mammography and MRI, Eur Radiol 28 (9) (2018) 3731–3741.
[56] N.D. Prionas, K.K. Lindfors, S. Ray, S.-Y. Huang, L.A. Beckett, W.L. Monsky, J. M. Boone, Contrast-enhanced Dedicated Breast CT: Initial Clinical Experience, Radiology 256 (3) (2010) 714–723.
[57] J. Uhlig, U. Fischer, L. Biggemann, J. Lotz, S. Wienbeck, Pre- and post-contrast versus post-contrast cone-beam breast CT: can we reduce radiation exposure while maintaining diagnostic accuracy? Eur Radiol 29 (6) (2019) 3141–3148.
[58] V. Ruth, D. Kolditz, C. Steiding, W.A. Kalender, Investigation of spectral performance for single-scan contrast-enhanced breast CT using photon-counting technology: A phantom study, Med. Phys. 47 (7) (2020) 2826–2837.
[59] A.K. Carton, J. Li, M. Albert, S. Chen, A.D.A. Maidment, Quantification for contrast-enhanced digital breast tomosynthesis. Quantification for contrast-enhanced digital breast tomosynthesis, 2006.
[60] R.A. Jong, M.J. Yaffe, M. Skarpathiotakis, R.S. Shumak, N.M. Danjoux, A. Gunesekara, D.B. Plewes, Contrast-enhanced Digital Mammography: Initial Clinical Experience, Radiology 228 (3) (2003) 842–850.
[61] G. Gennaro, A. Cozzi, S. Schiaffino, F. Sardanelli, F. Caumo, Radiation Dose of Contrast-Enhanced Mammography: A Two-Center Prospective Comparison, Cancers 14 (7) (2022) 1774, https://doi.org/10.3390/cancers14071774. PMID: 35406546 PMCID: PMC8997084.
[62] R.E. Hendrick, Radiation Doses and Risks in Breast Screening, Journal of Breast Imaging 2 (3) (2020) 188–200, https://doi.org/10.1093/jbi/wbaa016.
[63] P.A.K. Oliver, R.M. Thomson, Investigating energy deposition in glandular tissues for mammography using multiscale Monte Carlo simulations, Med. Phys. 46 (3) (2019) 1426–1436.
[64] A. Sarno, G. Mettivier, K. Bliznakova, A.M. Hernandez, J.M. Boone, P. Russo, Comparisons of glandular breast dose between digital mammography, tomosynthesis and breast CT based on anthropomorphic patient-derived breast phantoms, Physica Med. 97 (19) (2022) 50–58, https://doi.org/10.1016/j.ejmp.2022.03.016.
[65] I. Sechopoulos, S.S.J. Feng, C.J. D'Orsi, Dosimetric characterization of a dedicated breast computed tomography clinical prototype: Dedicated breast CT dosimetry, Med. Phys. 37 (8) (2010) 4110–4120.
[66] W.A. Kalender, D. Kolditz, C. Steiding, V. Ruth, F. Lück, A.-C. Rößler, E. Wenkel, Technical feasibility proof for high-resolution low-dose photon-counting CT of the breast, Eur Radiol 27 (3) (2017) 1081–1086.
[67] A. Hernandez, J. Boone, Average glandular dose coefficients for pendant-geometry breast CT using realistic breast phantoms, Med. Phys. 44 (10) (2017) 0094–2405, https://doi.org/10.1002/mp.12477.
[68] Y. Kyriakou, P. Deak, O. Langner, W.A. Kalender, Concepts for dose determination in flat-detector CT, Phys. Med. Biol. 53 (13) (2008) 3551–3566.
[69] A. Abuhaimed, J.M. Colin, O. Demirkaya, Influence of cone beam CT (CBCT) scan parameters on size specific dose estimate (SSDE): a Monte Carlo study, Physics in Medicine and Biology 64 (11) (2019) 115002, https://doi.org/10.1088/1361-6560/ab0bc8. PMID: 30822764.
[70] A.M. O'Connel, T.J. Marini, D.T.K. O'Connor, Cone-Beam Breast Computed Tomography: Time for a New Paradigm in Breast Imaging, Journal of Clinical Medicine 10 (2021) 5135, https://doi.org/10.3390/jcm10215135, PMCID: PMC8584471. PMID: 34768656.